


2002

Acceleration Element for Femtosecond Electron Pulse Compression

Bao-Liang Qian
Old Dominion University

Hani E. Elsayed-Ali
Old Dominion University, helsayed@odu.edu

Follow this and additional works at: https://digitalcommons.odu.edu/ece_fac_pubs

 Part of the [Atomic, Molecular and Optical Physics Commons](#), [Electromagnetics and Photonics Commons](#), [Nuclear Commons](#), [Optics Commons](#), and the [Plasma and Beam Physics Commons](#)

Repository Citation

Qian, Bao-Liang and Elsayed-Ali, Hani E., "Acceleration Element for Femtosecond Electron Pulse Compression" (2002). *Electrical & Computer Engineering Faculty Publications*. 112.
https://digitalcommons.odu.edu/ece_fac_pubs/112

Original Publication Citation

Qian, B. L., & Elsayed-Ali, H. E. (2002). Acceleration element for femtosecond electron pulse compression. *Physical Review E*, 65(4), 046502. doi:10.1103/PhysRevE.65.046502

Acceleration element for femtosecond electron pulse compression

Bao-Liang Qian^{1,2} and Hani E. Elsayed-Ali^{1,*}

¹*Department of Electrical and Computer Engineering, Old Dominion University, Norfolk, Virginia 23529-0256*

²*Department of Applied Physics, National University of Defense Technology, Changsha 410073, Hunan, People's Republic of China*

(Received 31 May 2001; published 2 April 2002)

An acceleration element is proposed for compressing the electron pulse duration in a femtosecond photoelectron gun. The element is a compact metal cavity with curved-shaped walls. An external voltage is applied to the cavity where a special electric field forms in such a way that the slow electrons in the electron pulse front are accelerated more than the fast electrons, and consequently the electron pulse duration will be compressed. The distribution of the electric field inside the acceleration cavity is analyzed for the geometry of the cavity. The electron dynamics in this acceleration cavity is also investigated numerically. Numerical results show that the electron pulse front and pulse duration can be improved by compensating for the effects of space charge and the initial energy spread of photoelectrons with a Lambertian angular distribution. Depending on the design parameters and the shape of the electron pulse, for a femtosecond electron gun with an electron energy of 30 keV, 10^3 electrons per pulse, and an electron drift length of 40 cm, the electron pulse duration can be reduced from 550 to 200 fs when using a compensating cavity with an average radius of 1.7 and 5.6 cm in length. Electron pulses shorter than 200 fs can be achieved if the length of the drift region is reduced.

DOI: 10.1103/PhysRevE.65.046502

PACS number(s): 41.75.Fr, 07.77.Ka, 41.90.+e, 41.85.Ja

I. INTRODUCTION

Generating picosecond and subpicosecond photoelectron pulses is required for operation of streak cameras [1–15] and for time-resolved electron diffraction [16–34]. Faster time resolution requires developing photoelectron pulses in the femtosecond regime. However, the technology for generating electron beams with pulse widths ~ 100 fs or less, electron energies of 10–50 keV with electron energy spread in the few eV range, and 10^3 – 10^4 electrons per pulse is not established. The photoelectron energy spread at the cathode and space-charge effects cause significant electron pulse broadening, and rapidly spread an initial femtosecond photoelectron pulse into the picosecond regime.

Generation of femtosecond electron pulses was demonstrated in the relativistic regime [35]. Relativistic electron pulses with a duration of 50 fs, electron energy of 2.6 MeV, and $(2-4.6) \times 10^8$ electrons per pulse was achieved by employing an electron pulse compression technology, in which a large electron energy spread was introduced and the electron pulse compression was achieved using a magnetic prism. However, for applications in streak cameras and electron diffraction, the electron energy is far below the relativistic regime and only a few eV or less energy spread can be tolerated. This makes magnetic electron pulse compression, as applied to a relativistic electron pulse with energy spread in the keV range, unfeasible. A method of temporal dispersion compression was suggested for the nonrelativistic case to produce 50 fs electron pulses, but to our knowledge, has not been experimentally implemented [9,10]. The effects of electron energy spread on electron pulse broadening can be reduced, to some extent, in the photocathode-to-mesh region by choosing a photocathode with a suitable work function close to the laser photon energy and applying a relatively

high acceleration electric field in the vicinity of the photocathode [2,4,14]. On the contrary, space-charge effects causing electron pulse broadening are more difficult to remove. Electron pulse broadening is often larger in the electron drift region than in the photocathode-to-mesh region [3,5,36–38]. For a photoactivated electron gun activated by a femtosecond laser pulse, the electron pulse broadens into the picosecond range in a short time as it propagates towards the anode and in the post-anode drift region. For the photoelectron gun configuration shown in Fig. 1(a), we have developed a simple fluid model to investigate the electron pulse broadening caused by photoelectron pulse spread and space-charge effects in both the photocathode-to-anode region and in the post-anode drift region [39]. Pulse broadening due to the initial photoelectron energy spread occurs mainly in the photocathode-to-anode region and is estimated to be ~ 150 fs for an initial photoelectron energy spread $\Delta E_0 = 0.2$ eV, $d = 3$ mm, and $V_0 = 30$ kV, where d is the photocathode-to-anode mesh spacing and V_0 is voltage applied to the photocathode, as shown in Fig. 1(a). However, pulse broadening due to space-charge effects becomes severe in the post-anode drift region, when the electron density is high, because of the large drift time in that region. Pulse broadening due to space-charge effects in the post-anode drift region can be expressed as [39]

$$\Delta t_{\text{sp}} = \frac{e^{1/2} m^{1/2} L^2 N}{4\sqrt{2} \pi V_0^{3/2} \epsilon_0 r_b^2}, \quad (1)$$

where $-e$ and m are the charge and mass of an electron, V_0 is the voltage applied between the cathode and the anode (mesh), r_b is the radius of the electron beam, L is the length of the drift region, N is the number of the electrons contained in the electron pulse, and ϵ_0 is the vacuum permittivity. Δt_{sp} is calculated to be 0.35 ps for $L = 40$ cm, $N = 1000$, $r_b = 0.45$ mm, and $V_0 = 30$ kV. Additional electron pulse

*FAX: (757) 683-3220; email address: helsayed@odu.edu

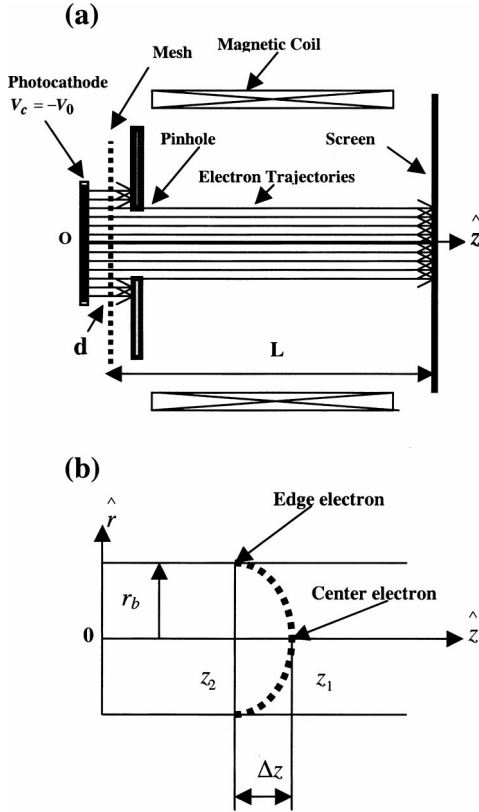


FIG. 1. (a) The configuration of a photoelectron gun. (b) A typical electron pulse front.

broadening occurs due to the energy spread of the photoelectrons at the surface of the photocathode. This calculation shows that the electron pulse broadening due to the space-charge effects and the initial photoelectron energy spread is an important issue in constructing an electron gun capable of delivering 1000 electrons per pulse over a 40 cm drift distance with a pulse width less than 200 fs.

The photoelectron energy spread and space-charge effects can make the beam diverge and electrons travel off axially, leading to electron pulse broadening. In general, an electron traveling exactly along the center axis will spend less time than an electron traveling off axially [9]. The electron pulse front develops into a shape resembling the shape shown in Fig. 1(b) [26] due to different off-axis velocities of electrons. Different off-axis velocities result from two factors. The first factor is the angular distribution of the photoelectrons emitted from the photocathode [40]. This factor can make the curvature shown in Fig. 1(b) contribute a time dispersion of about 150 fs for $\Delta E_0 = 0.2$ eV, $d = 3$ mm, and $V_0 = 30$ kV, assuming the angular distribution is Lambertian [14,26]. The second factor is the space-charge effects in the electron beam. In this case, the space-charge effects of the inner electrons in the electron pulse increase the radial components of velocities of the edge electrons, and lead to divergence of the electron beam. Similarly, an electron traveling along the center of the pulse front is faster along the axial direction than other electrons because it is accelerated by the space charge of the electrons following it. Consequently, for edge electrons the axial components of velocities are lower than for

electrons at or near the center that are drifting only along the axial direction. The electron pulse broadening caused by the space-charge effects is obtained from Eq. (1) [39].

In addition, if an axially directed accelerating electric field that increases off axially, or an axially directed decelerating electric field that decreases off axially, is generated in the drift region, the axial distances between the center electron and the edge electrons will be decreased. Thus, the electron pulse front can be improved and the temporal dispersion of the electron gun can be reduced. One should note that the whole electron pulse could be shortened as well using this kind of electric field because the electron pulse could be viewed to include a number of electron slices of the shape shown in Fig. 1(b) [26] due to the angular Lambertian distribution of photoelectrons and the space-charge effects. This electric field affects all the electron slices when the electron pulse passes through it.

We have recently investigated an electron dispersion-compensating element that could produce a decelerating electric field for electron pulse compression in femtosecond photoelectron guns [41]. However, the deceleration element previously investigated reduces the electron energy considerably and post acceleration is needed [41]. In addition, according to Eq. (1), space-charge effects become important when the electron energy (eV_0) is decreased. Consequently, electron pulse broadening by space charge limits pulse compression inside the deceleration element. Numerical calculations of the deceleration element indicate that the electron energy needs to be decreased from 30 to 16 keV inside the element to obtain the desired compression of the electron pulse duration [41]. Therefore, the design of the decelerating compression element requires careful trade off between the compression effect of the nonuniform electric field inside the element and the potential pulse broadening due to enhanced space-charge effects for the slowed electron pulse. The purpose of this paper is to introduce an acceleration element for electron pulse compression in femtosecond electron guns. The space-charge effects in this acceleration element are negligibly small. Therefore, the acceleration element is expected to be more effective than the deceleration element for compression of the electron pulse width. In addition, it offers the possibility of stacking several elements in cascade for achieving shorter electron pulses.

The remainder of the present paper is as follows. In Sec. II, the configuration of the compensating element and the basic formulation are given. In Sec. III, the equation of motion is solved to obtain the trajectories of the electrons in an electron pulse front and the results are given showing the compression of the electron pulse. The conclusions are stated in Sec. IV.

II. CONFIGURATION AND MODEL OF THE ACCELERATION ELEMENT

The basic configuration of the compensating element is shown in Fig. 2. The element is a metallic cylindrical cavity with a length L and a curve-shaped wall whose radius, $R(z)$, varies according to the relation:

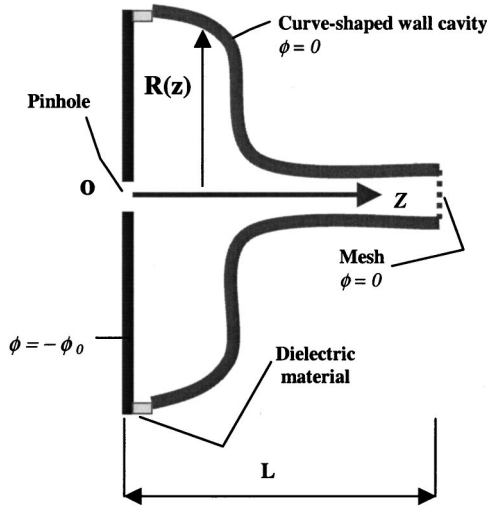


FIG. 2. The configuration of the acceleration element for a femtosecond electron gun.

$$R(z) = \begin{cases} R_0 + h \cos(k_0 z), & 0 \leq z \leq \pi/k_0 \\ R_0 - h & \pi/k_0 < z \leq L, \end{cases} \quad (2)$$

where R_0 is the average radius of the cavity, h is the variation amplitude of the cavity radius, and $z_0 = 2\pi/k_0$ is the period. Using these parameters one can easily control the shape of the cavity. On one side of the cavity, there is a pinhole through which the electron pulse can pass along the axial direction \hat{z} , and this side has an externally applied potential of $\phi = -\phi_0 < 0$, which is electrically insulated from the other sides of the cavity by an insulation material or vacuum gap. At the end of the cavity there is a fine mesh that can be used to guide the motion of the electrons. The thickness of the insulation material or vacuum gap should be much smaller than the length L of the cavity. In addition, the radius of the pinhole r_0 is assumed much smaller than the minimum radius of $R_0 - h$ of the cavity. The curve-shaped wall and mesh are both grounded. We will next discuss the interaction of the electron pulse with the electric field inside the cavity.

The potential distribution ϕ within the cavity can be described by the Poisson's equation in the cylindrical coordinates (r, θ, z) , which is written as

$$\frac{1}{r} \frac{\partial}{\partial r} \left(r \frac{\partial \phi}{\partial r} \right) + \frac{\partial^2 \phi}{\partial z^2} = 0. \quad (3)$$

where $\partial/\partial\theta = 0$ because of the azimuthal symmetry. The fine mesh is treated as a solid metallic sheet, and the effects of the insulation material and the pinhole whose radius r_0 is much smaller than the minimum radius $R_0 - h$ of the cavity are ignored. Using the boundary conditions of $\phi(z=0) = -\phi_0 < 0$ and $\phi(z=L) = 0$, one can solve Eq. (3) and obtain the potential distribution ϕ , which is written as

$$\phi = \sum_{n=1}^{\infty} A_n \sin(k_n z) I_0(k_n r) + \phi_0 \frac{z-L}{L}, \quad (4)$$

where $I_0(x)$ is the modified Bessel function of zero order of the first kind, A_n with $n=1,2,3,\dots$, are constants that need to be determined, and $k_n = n\pi/L$ with $n=1,2,3,\dots$ are wave numbers of the harmonic components of the potential distribution. Using the boundary condition of $\phi[r=R(z)] = 0$ in Eq. (4), multiplying Eq. (4) by $\sin(k_m z)$, and then integrating from $z=0$ to $z=L$, one can obtain

$$\sum_{n=1}^{\infty} D_{mn} A_n = B_m, \quad m=1,2,3,\dots, \quad (5)$$

where

$$D_{mn} = \frac{k_m}{\phi_0} \int_0^L \sin(k_m z) \sin(k_n z) I_0(k_n R(z)) dz, \quad m, n=1,2,3,\dots \quad (6)$$

and

$$B_m = 1. \quad (7)$$

The constants A_n can be determined from Eq. (5) using numerical calculations.

The components of the electric field in the cavity are expressed as

$$E_r = -\frac{\partial \phi}{\partial r} = -\sum_{n=1}^{\infty} A_n k_n \sin(k_n z) I_1(k_n r) \quad (8)$$

and

$$E_z = -\frac{\partial \phi}{\partial z} = -\sum_{n=1}^{\infty} A_n k_n \cos(k_n z) I_0(k_n r) - \frac{\phi_0}{L}, \quad (9)$$

where E_r is the radial component of the electric field, E_z is the axial component of the electric field, $I_1(x)$ is the modified Bessel function of the first order of the first kind.

The compensating element described in Fig. 2 should be immersed in a relatively strong axial guide magnetic field B to compensate for the divergence due to E_r . The parameters of ϕ_0 , L , R_0 , h , and k_0 can be adjusted in order to achieve the desired compensation results. Equations (8) and (9) are numerically evaluated to obtain the distribution of the electric field in the cavity. For the sake of convenience, dimensionless variables are used in the calculations. The normalization variables are $E_0 = \phi_0/L$ and L .

Figure 3 shows the axial electric field E_z as a function of the distance r from the center of the cylindrical cavity for $R_0/L = 0.3$, $h_0/L = 0.2$, and $L/z_0 = 2.5$ in the cases of $z/L = 0.10, 0.15$, and 0.20 . The axial component of the electric field E_z is negative and thus provides an accelerating field for electrons entering the pinhole. The amplitude of E_z increases with r for $z/L < 0.15$, and decreases with r for $z/L > 0.20$. Therefore, the edge electrons in the electron front are accelerated more than the center electron in the case of $z/L < 0.15$, and electron pulse compression in the acceleration cavity occurs. On the contrary, the center electron will be accelerated more than the edge electrons for $z/L > 0.20$,

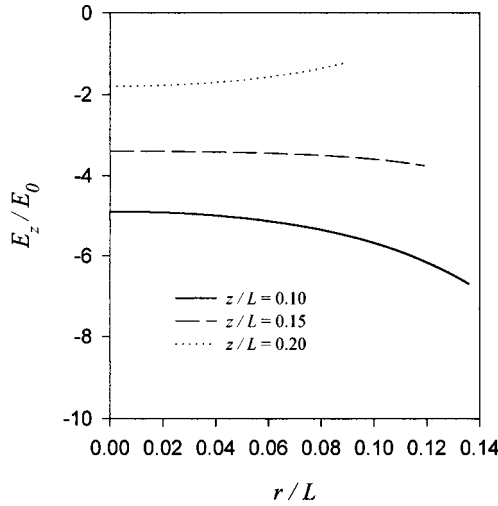


FIG. 3. The axial electric field E_z in the compensating element as a function of r for $R_0/L=0.3$, $h_0/L=0.2$, and $L/z_0=2.5$ in the cases of $z/L=0.10$, 0.15 , and 0.20 .

which broadens the electron pulse. Fortunately, the amplitude of E_z decreases rapidly with z when $r/L < 0.16$, which makes the broadening effect small. It is also shown later, that the broadening effect will not prevent the cavity from improving the electron pulse front and compressing the photoelectron pulse width because the electric field in this region is too small to alter the compressing function of the cavity.

Figure 4 shows the radial electric field E_r as a function r for $R_0/L=0.3$, $h_0/L=0.2$, and $L/z_0=2.5$ in the cases of $z/L=0.05$, 0.10 , and 0.15 . As can be seen from Fig. 4, E_r is negative, and its amplitude increases with both r and z when $z/L < 0.15$ and $r/L < 0.10$. The divergence effects of E_r on the electrons can be efficiently compensated for by an axial magnetic field B .

An efficient way to investigate the physics of the compensating element is to depict the trajectories of the electrons contained in the electron pulse front when the pulse passes

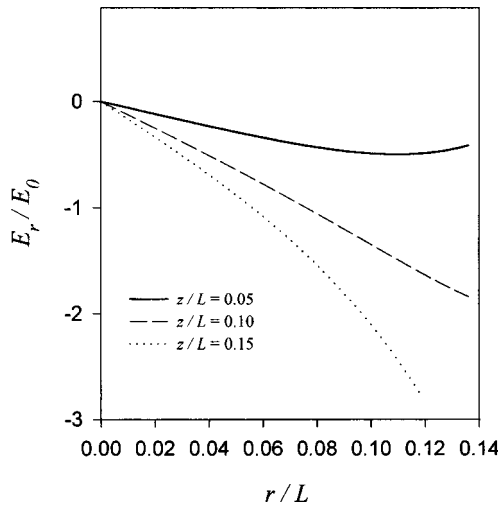


FIG. 4. The radial electric field E_r in the compensating element as a function of r for $R_0/L=0.3$, $h_0/L=0.2$, and $L/z_0=2.5$ in the cases of $z/L=0.05$, 0.10 , and 0.15 .

through the element. We next formulate a model by which the electron trajectories of the electron pulse front can be obtained. It is appropriate to assume that the length L of the compensating cavity is short enough to neglect the self-space-charge effects of the electron beam [39]. In this case, the motion of the electrons will be only in the externally applied constant magnetic field B and the electric field $\vec{E} = E_r\hat{r} + E_z\hat{z}$ in the compensating cavity, which is given by Eqs. (8) and (9). The components of the equation of motion for an electron are written as

$$\frac{dv_r}{dt} = \frac{v_\theta^2}{r} - \frac{e}{m}[E_r + v_\theta B], \quad (10)$$

$$\frac{dv_\theta}{dt} = \frac{eBv_r}{m} - \frac{v_r v_\theta}{r}, \quad (11)$$

and

$$\frac{dv_z}{dt} = -\frac{eE_z}{m}, \quad (12)$$

where $-e$ and m are electron charge and mass, $\vec{v} = v_r\hat{r} + v_\theta\hat{\theta} + v_z\hat{z}$ is the electron velocity in cylindrical coordinates, and E_r and E_z are given by Eqs. (8) and (9). Other useful relations are

$$\frac{dr}{dt} = v_r, \quad (13)$$

$$\frac{d\theta}{dt} = \frac{v_\theta}{r}, \quad (14)$$

and

$$\frac{dz}{dt} = v_z. \quad (15)$$

Equations (10)–(15) can be used to investigate the motion of the electrons in the compensating cavity. There are no analytical solutions to Eqs. (10)–(15), and numerical solutions are necessary to obtain the electron trajectories. However, one can understand the effects of the axially applied constant magnetic field using these equations. The radial electric field $E_r < 0$ can make the electron beam diverge. The divergence sources come from two terms in Eq. (10). One term is $v_\theta^2/r > 0$, and the other is $-eE_r/m > 0$ with $E_r < 0$ observed from Fig. 4. These two terms result in an increase in the radial velocity v_r , which is a divergence velocity component. In the following calculations, we assume that $v_r > 0$ and $v_\theta = 0$ at $t = 0$, thus $v_\theta > 0$ at $t > 0$, which can be deduced from Eq. (11). The last term in Eq. (10) is therefore $-ev_\theta B/m < 0$ with $B > 0$, which can compensate for the divergence effects of $v_\theta^2/r > 0$ and $-eE_r/m > 0$ in Eq. (10). In general, the length of the compensating element investigated in this paper is around 6 cm for an initial electron energy of 30 keV, which corresponds to an electron velocity of about 0.8×10^{10} cm/s (see Sec. III). Therefore, the transit time of

an electron in the compensating element is $T_t = L/v_z \approx 6 \text{ cm}/(0.8 \times 10^{10} \text{ cm/s}) \approx 0.75 \text{ ns}$. In addition, the cyclotron frequency of the electron in the constant magnetic field is $\omega_c = eB/m$, and the gyration period is $T_c = 2\pi/\omega_c = 2\pi n/eB \approx 0.29 \text{ ns}$ for $B = 200 \text{ G}$, which is a reasonable design value of magnetic field for an electron gun. One should note that $T_t = 0.75 \text{ ns} > T_c = 0.29 \text{ ns}$, which means that the electron gyration is not slow, compared with the electron transit time. This shows that the 200 G axially applied magnetic field is sufficient to compensate for the beam divergence caused by the radial electric field $E_r < 0$.

III. NUMERICAL RESULTS

In this section we describe the results of a numerical solution of Eqs. (10)–(15) to further explore the physics of the compensating element described in Fig. 2. We assume that the electron pulse is azimuthally symmetric. Therefore, all the edge electrons in the electron front have the same velocity and trajectory. We only consider two kinds of electrons contained in the electron pulse front, i.e., the center electron and the edge electrons as shown in Fig. 1(b). It is convenient to use dimensionless variables to treat these equations. In addition to $r_c = mc/eB$ and $E_0 = \phi_0/L$, the physical quantities involved in the following numerical solution are the radius r_b of the electron beam or, equivalently, the radial position $r = r_b$ of the edge electrons in the electron pulse front, the radial position $r = r_{\text{cen}} = 0$ of the center electron, the axial position $z = z_1$ and axial velocity $v_z = v_{z1}$ of the center electron, the axial position $z = z_2$ and axial velocity $v_z = v_{z2}$ of the edge electrons, the axial distance $\Delta z = z_1 - z_2$ and the axial velocity difference $\Delta v_z = v_{z1} - v_{z2}$ between the center electron and the edge electrons, the average initial drift velocity v_0 of the electrons at the entrance of the compensating cavity, the average initial kinetic energy $\varepsilon = mv_0^2/2$ of the electrons, the initial electron energy spread $\Delta\varepsilon$ of the electron pulse at the entrance of the cavity, and the cyclotron frequency $\omega_c = eB/m$ of the electrons in the magnetic field B .

In addition, at the entrance of the compensating cavity, the center electron is initially at $(r, z) = (r_{\text{cen}}, z_1) = (0, z_{10})$ with $z_{10} > 0$, and the edge electrons are initially at $(r, z) = (r_b, z_2) = (r_b, z_{20}) = (r_b, 0)$. Therefore, the axial distance between the center electron and the edge electrons is initially $\Delta z = \Delta z_0 = z_{10}$. The radius r_0 of the pinhole at the entrance of the compensating cavity is assumed to be larger than the initial electron beam radius r_b . At the axial position $z = L$, the electron reaches the end of the compensating cavity. In order to show the effects of electron energy spread on the electron pulse front, we will investigate the case in which the initial kinetic energy difference between the center electron and the edge electrons at the entrance of the compensating cavity is equal to the energy spread $\Delta\varepsilon$. Moreover, the initial velocity \vec{v}_0 of the electrons at the entrance of the compensating cavity takes the form of $\vec{v}_0 = v_0[\sin(\theta_0)\hat{r} + \cos(\theta_0)\hat{z}]$, where θ_0 is the velocity divergence angle. The center electron is assumed to have $\theta_0 = \theta_{01} = 0$, but for the edge electrons $\theta_0 = \theta_{02} > 0$, where θ_{01} and θ_{02} refer to the velocity divergence angles of center electron and edge electrons, re-

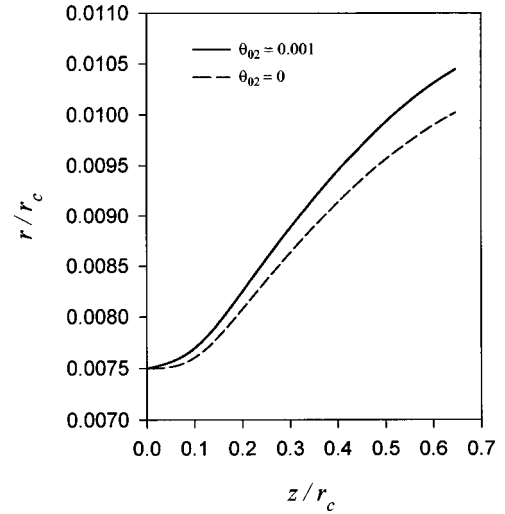


FIG. 5. The radial position r of the edge electrons in the electron pulse front as a function of the axial position z for $r_b/r_c = 0.0075$, $z_{20} = 0$, $v_0/c = 1/3$, $R_0/L = 0.3$, $h/L = 0.2$, $L/z_0 = 2.5$, $L/r_c = 0.65$, and $E_0/cB = 0.04$ in the cases of $\theta_{02} = 0$ and $\theta_{02} = 0.001$.

spectively. It is worth noting that our model does not include the details of the shape of the electron pulse front and the initial axial distance Δz_0 between the center electron and the edge electrons. The actual shape of the electron pulse front depends on the electron dynamics before the entrance of the compensating cavity.

Figure 5 shows the radial position r of the edge electrons in the electron pulse front as a function of the axial position z for $r_b/r_c = 0.0075$, $z_{20} = 0$, $v_0/c = 1/3$, $R_0/L = 0.3$, $h/L = 0.2$, $L/z_0 = 2.5$, $L/r_c = 0.65$, and $E_0/cB = 0.04$ in the cases of $\theta_{02} = 0$ and $\theta_{02} = 0.001$. It can be seen from Fig. 5 that the beam radius r_b varies from $0.0075r_c$ to about $0.0104r_c$ in the case of $\theta_{02} = 0.001$ when the electron pulse passes through the compensating element, and the beam radius r_b changes from $0.0075r_c$ to about $0.01r_c$ in the case of $\theta_{02} = 0$. Therefore, the effect of the radial electric field E_r on the beam divergence is small in the case of a constant axially applied magnetic field B .

The compensating effect can be clearly seen from Fig. 6, where we have plotted the axial velocity difference $\Delta v_z = v_{z1} - v_{z2}$ between the center electron and the edge electrons in the electron pulse front as a function of z for $r_b/r_c = 0.0075$, $z_{10}/r_c = 0.00040$, $z_{20} = 0$, $\theta_{01} = 0$, $\theta_{02} = 0.001$, $v_0/c = 1/3$, $\Delta\varepsilon/\varepsilon = 0.000036$, $R_0/L = 0.3$, $h/L = 0.2$, $L/z_0 = 2.5$, $L/r_c = 0.65$, and $E_0/cB = 0.04$. At the entrance of the cavity, the velocity of the center electron is larger than the velocity of the edge electrons, i.e., $\Delta v_z = v_{z1} - v_{z2} > 0$. However, Δv_z decreases with z and quickly becomes negative at $z/r_c > 0.01$, which means that the electron pulse front is improved and the pulse is compressed. In addition, Δv_z remains a negative constant in the case of $z/r_c > 0.2$ because the electric field in this region is too small to affect the motion of the electrons.

The improvement in the electron front and compression of the electron pulse can also be observed in Fig. 7, where we have plotted the axial distance $\Delta z = z_1 - z_2$ between the center electron and the edge electrons in the electron pulse front

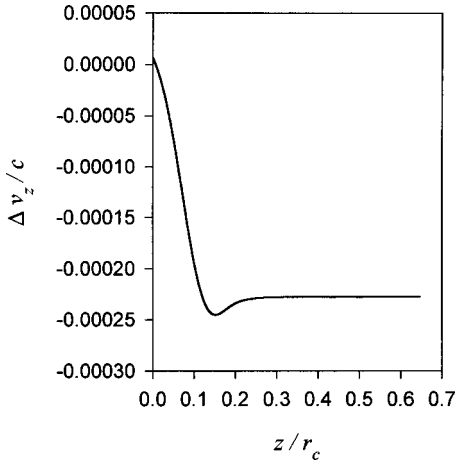


FIG. 6. The axial velocity difference $\Delta v_z = v_{z1} - v_{z2}$ between the center electron and the edge electrons in the electron pulse front as a function of z for $r_b/r_c = 0.0075$, $z_{10}/r_c = 0.00040$, $z_{20} = 0$, $\theta_{01} = 0$, $\theta_{02} = 0.001$, $v_0/c = 1/3$, $\Delta\varepsilon/\varepsilon = 0.000036$, $R_0/L = 0.3$, $h/L = 0.2$, $L/z_0 = 2.5$, $L/r_c = 0.65$, and $E_0/cB = 0.04$.

as a function of time t for the same parameters as used in Fig. 6 for different initial axial distances of $\Delta z_0/r_c = 0.00045$, 0.00040 , and 0.00035 . As can be seen from Fig. 7, the axial distance between the center electron and the edge electrons decreases abruptly with time t due to the strong compensating electric field experienced by the electron pulse in the cavity. This is easily understood using the data shown in Figs. 6, where the curve shows the axial velocity difference Δv_z between the center electron and the edge electrons. As shown in Fig. 7, the values of Δz become very small at the end of the cavity, which means that the edge electrons have caught up with the center electron, and consequently the electron pulse duration is compressed.

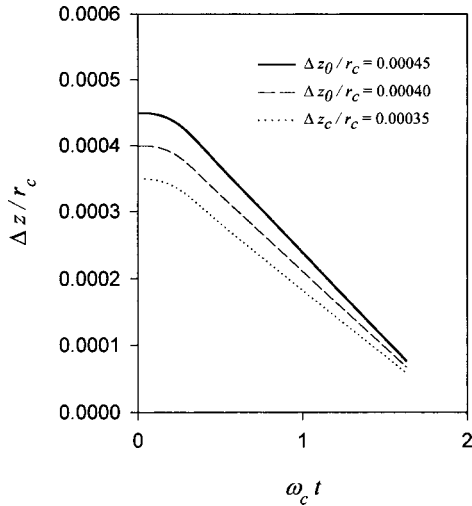


FIG. 7. The axial distance $\Delta z = z_1 - z_2$ between the center electron and the edge electrons in the electron pulse front as a function of time t for $r_b/r_c = 0.0075$, $\theta_{01} = 0$, $\theta_{02} = 0.001$, $v_0/c = 1/3$, $\Delta\varepsilon/\varepsilon = 0.000036$, $R_0/L = 0.3$, $h/L = 0.2$, $L/z_0 = 2.5$, $L/r_c = 0.65$, and $E_0/cB = 0.04$ in the cases of different initial axial distances of $\Delta z_0/r_c = 0.00045$, 0.00040 , and 0.00035 .

The numerical results obtained above can be used to design a compensating cavity. However, a long compensating device should be avoided because a long electron beam drift distance will result in a considerable electron pulse broadening due to space-charge effects. A compensating cavity of less than 6 cm in length is suitable for a 200 fs electron gun with 10^3 electrons per pulse because in this case the space-charge pulse broadening in the cavity Δt_{sp} is less than 10 fs for a beam radius of $r_b = 0.45$ mm and average electron drift kinetic energy at the cavity entrance of $\varepsilon = 30$ keV, according to Eq. (1). In addition, the radius of the compensating cavity should also be as small as possible in order to focus the distribution of the electric field to meet the compensating requirements inside the cavity. The results shown in Figs. 5–7 indicate that appropriate design parameters of the compensating cavity can be $L = 5.6$ cm, $R_0 = 1.7$ cm, $h = 1.1$ cm, $z_0 = 2.2$ cm, $\phi_0 = 14$ kV, and $B = 200$ G. These design parameters are applied for a photoelectron gun with an electron energy of 30 keV, a space-charge-caused electron energy spread of ~ 1.1 eV, an electron beam radius ~ 0.6 mm at the compensating cavity, and 10^3 electrons per pulse. In the example we gave earlier, a 50 fs photoelectron pulse at the photocathode broadened by its initial energy spread at the photocathode, the angular Lambertian distribution, and space-charge effects to $\Delta t_p \approx 550$ fs [39]. For these design parameters, the electron pulse front can be improved considerably and the electron pulse duration can be reduced by as much as $\Delta z_0/v_0 \approx 350$ fs according to Fig. 7. In this case, the electron pulse duration may reach a value of 200 fs ($= 550 - 350$ fs). The insulation gap between the electrode at $-\phi_0$ and the grounded cavity can be a few mm, enough to hold off breakdown in vacuum. The model ignores this distance, which is valid when the length of the cavity is much larger than the isolation gap.

IV. CONCLUSIONS

An acceleration element for improving the electron pulse front and compressing the pulse duration has been investigated. This compensating element is a compact metal cavity with curved-shaped walls and can be used in developing femtosecond photoelectron guns for applications in streak cameras and time-resolved electron diffraction. An external voltage is applied to the cavity where a special electric field forms in such a way that the slow electrons in the electron pulse front are accelerated more than the fast electrons, and consequently the electron pulse duration will be compressed. The distribution of the electric field inside the acceleration cavity is analyzed on the basis of the geometry of the cavity. The electron dynamics in this acceleration cavity is also investigated. Numerical results show that the electron pulse duration is reduced due to compensating for the initial angular Lambertian distribution of photoelectrons, initial photoelectron energy spread, and space-charge effects in the electron drift region.

In order to avoid space-charge effects on the electron pulse and to focus the distribution of the electric field inside

the cavity for efficient compensation, the length and diameter of the cavity should be kept short. Depending on the design parameters and the shape of the electron pulse, for a typical femtosecond electron gun with an electron energy of 30 keV and 10^3 electrons per pulse, the electron pulse duration may be reduced by as much as 350 fs when using a compensating cavity with an average radius of 1.7 cm and 5.6 cm in length.

ACKNOWLEDGMENTS

This work was supported by the National Science Foundation through Grant Nos. DMR-9988669 and DMR-0116015 and the U.S. Department of Energy through Grant No. DE-FG02-97ER45625. The research by B.-L. Qian was supported by the National University of Defense Technology in P. R. China.

-
- [1] D. J. Bradley and W. Sibbett, *Appl. Phys. Lett.* **27**, 382 (1975).
- [2] V. N. Platonov and M. Ya. Shchelev [*Sov. Phys. Tech. Phys.* **24**, 954 (1979)].
- [3] H. Niu and W. Sibbett, *Rev. Sci. Instrum.* **52**, 1830 (1981).
- [4] H. Niu, W. Sibbett, and M. R. Baggs, *Rev. Sci. Instrum.* **53**, 563 (1982).
- [5] W. Sibbett, H. Niu, and M. R. Baggs, *Rev. Sci. Instrum.* **53**, 758 (1982).
- [6] K. Kinoshita, M. Ito, and Y. Suzuki, *Rev. Sci. Instrum.* **58**, 932 (1987).
- [7] A. Finch, Y. Liu, H. Niu, W. Sibbett, W. E. Slent, D. R. Walker, Q. L. Yang, and H. Zhang, *Proc. SPIE* **1032**, 622 (1988).
- [8] J. Ihlemann, A. Helmbold, and H. Staerk, *Rev. Sci. Instrum.* **59**, 2502 (1988).
- [9] H. Niu, V. P. Degtyareva, V. N. Platonov, A. M. Prokhorov, and M. Ya. Schelev, *Proc. SPIE* **1032**, 79 (1988).
- [10] H. Niu, H. Zhang, Q. L. Yang, Y. P. Liu, Y. C. Wang, Y. A. Reng, and J. L. Zhou, *Proc. SPIE* **1032**, 472 (1988).
- [11] M. M. Murnane, H. C. Kapteyn, and R. W. Falcone, *Appl. Phys. Lett.* **56**, 1948 (1990).
- [12] M. D. Duncan, R. Mahon, L. L. Tankersley, and J. Reintjes, *Appl. Opt.* **29**, 2369 (1990).
- [13] R. Shepherd, R. Booth, D. Price, M. Bowers, D. Swan, J. Bonlie, B. Young, J. Dunn, B. White, and R. Stewart, *Rev. Sci. Instrum.* **66**, 719 (1995).
- [14] Z. Chang, A. Rundquist, M. M. Murnane, H. C. Kapteyn, X. Liu, B. Shan, J. Liu, L. Niu, M. Gong, and X. Zhang, *Appl. Phys. Lett.* **69**, 133 (1996).
- [15] A. Maksimchuk, M. Kim, J. Workman, G. Korn, J. Squier, D. Du, D. Umstadter, and G. Mourou, *Rev. Sci. Instrum.* **67**, 697 (1996).
- [16] G. Mourou and S. Williamson, *Appl. Phys. Lett.* **41**, 44 (1982).
- [17] S. Williamson, G. A. Mourou, and J. M. C. Li, *Phys. Rev. Lett.* **52**, 2364 (1984).
- [18] H. E. Elsayed-Ali and G. A. Mourou, *Appl. Phys. Lett.* **52**, 103 (1988).
- [19] H. E. Elsayed-Ali and J. W. Herman, *Rev. Sci. Instrum.* **61**, 1636 (1990).
- [20] H. E. Elsayed-Ali and J. W. Herman, *Appl. Phys. Lett.* **57**, 1508 (1990).
- [21] J. W. Herman and H. E. Elsayed-Ali, *Phys. Rev. Lett.* **68**, 2952 (1992).
- [22] J. W. Herman and H. E. Elsayed-Ali, *Phys. Rev. Lett.* **69**, 1228 (1992).
- [23] J. W. Herman, H. E. Elsayed-Ali, and E. A. Murphy, *Phys. Rev. Lett.* **71**, 400 (1993).
- [24] J. W. Herman and H. E. Elsayed-Ali, *Phys. Rev. B* **49**, 4886 (1994).
- [25] M. Aeschliman, E. Hull, J. Cao, C. A. Schmuttenmaer, L. G. Jahn, Y. Gao, H. E. Elsayed-Ali, D. A. Mantell, and M. R. Scheinfein, *Rev. Sci. Instrum.* **66**, 1000 (1995).
- [26] P. M. Weber, S. D. Carpenter, and T. Lucza, *Proc. SPIE* **2521**, 23 (1995).
- [27] J. R. Thompson, P. M. Weber, and P. J. Estrup, *Proc. SPIE* **2521**, 113 (1995).
- [28] H. E. Elsayed-Ali and P. M. Weber, in *Time-Resolved Diffraction*, edited by J. R. Helliwell and P. M. Rentzepis (Oxford University Press, Oxford, 1997), Chap. 12, pp. 284–322.
- [29] J. C. Williamson, J. Cao, H. Ihee, H. Frey, and A. H. Zewail, *Nature (London)* **386**, 159 (1997).
- [30] H. Ihee, J. Cao, and A. H. Zewail, *Chem. Phys. Lett.* **281**, 10 (1997).
- [31] J. Cao, H. Ihee, and A. H. Zewail, *Chem. Phys. Lett.* **290**, 1 (1998).
- [32] M. Ya. Schelev, G. I. Bryukhnevich, V. I. Lozovoi, M. A. Monastyrski, A. M. Prokhorov, A. V. Smirnov, and N. S. Vorobiev, *Opt. Eng.* **37**, 2249 (1998).
- [33] X. L. Zeng, Bo Lin, I. El-Kholy, and H. E. Elsayed-Ali, *Surf. Sci.* **439**, 95 (1999).
- [34] X. L. Zeng, Bo Lin, I. El-Kholy, and H. E. Elsayed-Ali, *Phys. Rev. B* **59**, 14 907 (1999).
- [35] P. Kung, H. C. Lihn, and H. Wiedemann, *Phys. Rev. Lett.* **73**, 967 (1994).
- [36] R. Clauberg and A. Blacha, *J. Appl. Phys.* **65**, 4095 (1989).
- [37] J. P. Girardeau-Montaut and C. Girardeau-Montaut, *J. Appl. Phys.* **65**, 2889 (1989).
- [38] C. Girardeau-Montaut, J. P. Girardeau-Montaut, and H. Leboutet, *Appl. Phys. Lett.* **55**, 2556 (1989).
- [39] Bao-Liang Qian and Hani E. Elsayed-Ali, *J. Appl. Phys.* **91**, 462 (2002).
- [40] B. L. Henke, J. Liesegang, and S. D. Smith, *Phys. Rev. B* **19**, 3004 (1979).
- [41] Bao-Liang Qian and Hani E. Elsayed-Ali, *Rev. Sci. Instrum.* **72**, 3507 (2001).